Small molecule inhibitor of OGG1 blocks oxidative DNA damage repair at telomeres and potentiates Methotrexate anticancer effects

Juan Miguel Baquero
Spanish National Cancer Research Centre https://orcid.org/0000-0002-6488-7742
Carlos Benítez-Buelga (carlos.benitez-buelga@scilifelab.se)
Karolinska Institutet
Varshni Rajagopal
Karolinska Institutet
Zhao Zhenjun
Karolinska Institutet
Raúl Torres-Ruiz
Centro Nacional de Investigaciones Oncologicas
Sarah Mueller
Karolinska Institutet
Bishoy Magdi Fekry Hanna
Karolinska Institutet
Olga Loseva
Karolinska Institutet
Olov Wallner
Karolinska Institutet
Maurice Michel
Karolinska Institutet
Sandra Rodríguez-Perales
Centro Nacional de Investigaciones Oncologicas
Helge Gad
Karolinska Institutet
Torkild Visnes
SINTEF
Thomas Helleday
Karolinska Institutet
Javier Benítez
Centro Nacional de Investigaciones Oncologicas
Ana Osorio

Centro Nacional de Investigaciones Oncologicas

Research

Keywords: Oxidative stress, oxidative DNA damage, OGG1 inhibition, telomere dysfunction, genome instability

Posted Date: August 24th, 2020

DOI: https://doi.org/10.21203/rs.3.rs-57290/v2

Version of Record: A version of this preprint was published at Scientific Reports on February 10th, 2021.
See the published version at https://doi.org/10.1038/s41598-021-82917-7.

Title: Small molecule inhibitor of OGG1 blocks oxidative DNA damage repair at telomeres and potentiates Methotrexate anticancer effects

Author names: Juan Miguel Baquero[1,†], Carlos Benítez-Buelga[2,†,*],Varshni Rajagopal[2], Zhao Zhenjun[2], Raúl Torres-Ruiz[3,4], Sarah Mueller[2], Bishoy Magdi Fekry Hanna[2], Olga Loseva[2], Olov Wallner[2], Maurice Michel[2], Sandra Rodríguez-Perales[3], Helge Gad[2,5], Torkild Visnes[6], Thomas Helleday[2,5], Javier Benítez[1,7,8] and Ana Osorio[1,7,*]

Addresses:

[1] Human Genetics Group, Human Cancer Genetics Programme, Spanish National Cancer Research Centre (CNIO), Madrid, 28029, Spain

[2] Science for Life Laboratory, Department of Oncology-Pathology, Karolinska Institutet, Solna, 17121, Sweden

[3] Molecular Cytogenetics Group, Human Cancer Genetics Programme, Spanish National Cancer Research Centre, Madrid (CNIO), 28029, Spain

[4] Josep Carreras Leukemia Research Institute, Department of Biomedicine, School of Medicine, University of Barcelona, Barcelona, 08036, Spain

[5] Weston Park Cancer Centre, Department of Oncology and Metabolism, University of Sheffield, Sheffield S10 2RX, United Kingdom

[6] Department Biotechnology and Nanomedicine, SINTEF Industry, Trondheim, N-7465, Norway

[7] Spanish Network on Rare Diseases (CIBERER), Madrid, 28029, Spain

[8] Human Genotyping-CEGEN Unit, Human Cancer Genetics Programme, Spanish National Cancer Research Centre, Madrid (CNIO), 28029, Spain

*To whom correspondence should be addressed. Tel: +34 91 732 8002; Fax: +34912246980; Email: aosorio@cnio.es. Correspondence may also be addressed to Carlos Benítez-Buelga. Tel: +46700248453; Email: carlos.benitez-buelga@scilifelab.se

†The authors wish it to be known that, in their opinion, the first two authors should be regarded as joint First Authors.

ABSTRACT

Background: The most common oxidative DNA lesion is 8-oxoguanine (8-oxoG) which is mainly recognized and excised by the glycosylase OGG1, initiating the Base Excision Repair (BER) pathway. Telomeres are particularly sensitive to oxidative stress which disrupts telomere homeostasis triggering genome instability.

Methods: We used U2OS OGG1-GFP osteosarcoma cell line to study the role of OGG1 at the telomeres in response to oxidative stress. Next, we investigated the effects of inactivating pharmacologically the BER during oxidative stress (OS) conditions by using a specific small molecule inhibitor of OGG1 (TH5487) in different human cell lines.

Results: We have found that during OS, TH5487 effectively blocks BER initiation at telomeres causing accumulation of oxidized bases at this region, correlating with other phenotypes such as telomere losses, micronuclei formation and mild proliferation defects. Besides, the antimetabolite Methotrexate synergizes with TH5487 through induction of intracellular ROS formation, which potentiates TH5487 mediated telomere and genome instability in different cell lines.

Conclusions: Our findings demonstrate that OGG1 is required to protect telomeres from OS and present OGG1 inhibitors as a tool to induce oxidative DNA damage at telomeres, with the potential for developing new combination therapies for cancer treatment.

KEYWORDS

Oxidative stress, oxidative DNA damage, OGG1 inhibition, telomere dysfunction, genome instability

BACKGROUND

Telomeres are nucleoprotein structures that protect the ends of linear eukaryotic chromosomes. In humans, telomeric DNA is commonly 10–15 kb and is composed of tandemly 5'-(TTAGGG) n-3' hexanucleotide repeats that are coated by the telomere shelterin complex (1,2). Functional telomeres maintain genome stability by preventing chromosomal ends from being recognized as DNA strand breaks (3). On the other hand, dysfunctional telomeres, emanating from the loss of telomeric repeats and/or the loss of sheltering protection, are recognized by many DNA damage response proteins, including the

phosphorylated H2A histone family member X at serine 139 (γH2AX) or the p53-binding protein 1 (53BP1), that form telomere dysfunction-induced foci (TIF) and lead to genomic instability, cell proliferation defects or apoptosis (4,5). Cancer cells are characterized by preserving stable telomere length, thereby conferring cell immortality (6). In consequence, the induction of telomeric instability is considered as a potential therapeutic strategy for cancer treatment (7).

Oxidative DNA damage is generated by reactive oxygen species (ROS) and constitutes the majority of DNA damage in human cells (8). Several lines of evidence indicate that telomeres are particularly sensitive to oxidative stress (9,10). Considering that guanine has the lowest redox potential among canonical nucleobases, the high incidence of guanine residues at the telomeric DNA sequence makes telomeres a potential hotspot for oxidative DNA damage (11). During oxidative stress, 8-oxoguanine (8-oxoG) is the most common base lesion, which can be converted into single or double-strand breaks (SSBs or DSBs), if it is not repaired correctly, or can be mutagenic by GC-TA transversions (12). At telomeres, 8-oxoG decreases the binding of the shelterin complex (13,14), leading potentially to telomere shortening, uncapping and finally telomere crisis (14–16). This is a cellular state characterized by extensive genomic instability, including translocations, amplifications, and deletions related to aging-induced processes and cancer (17).

The Base Excision Repair (BER) pathway is the main responsible mechanism for removing oxidized nucleotides from DNA, and it is active at telomeres (18,19). BER can be initiated by eleven different DNA glycosylases that recognize and excise specific base lesions. In the case of BER initiation due to 8-oxodG excision by OGG1, the resulting abasic sites is cleaved by an apurinic/apyrimidinic endonuclease (APE1), that will generate an nucleotide gap containing a 3′-hydroxyl end. In short-patch BER the nucleotide gap is filled up with the correct nucleotide by polymerase β (POLB) and sealed by DNA ligase III (LIG3), in a process mediated by the scaffold protein X-ray repair cross-complementing 1 (XRCC1). (20,21). In human cells, 8-oxoG is mainly excised by 8-oxoG DNA glycosylase 1 (OGG1), which removes 8-oxoG opposite cytosine in double-stranded DNA. This enzyme is necessary to preserve telomere integrity, especially under oxidative stress conditions (14,16,22).

Fouquerel et al., (2019) have recently proven that acute 8-oxoG telomeric formation in cells lacking functional OGG1 leads to telomere fragility, while a chronic 8-oxoG exposure results into telomere shortening, replication stress at telomeres, telomere losses and postmitotic defects such as micronuclei formation, anaphase bridge formation, chromosome fusions and proliferation defects (16).

The recently developed OGG1 inhibitor TH5487 has proven to bind efficiently to the catalytic site of OGG1 blocking its enzymatic activity (23). We hypothesized that OGG1 inhibition may recapture the phenotypic telomeric defects previously observed in OGG1 depleted cells (16), representing an attractive and unexplored opportunity for compromising telomere integrity in cells exposed to high ROS levels. Furthermore, OGG1 inhibitors may potentiate the telomere instability associated with conventional chemotherapeutic agents, increasing its therapeutic effect.

In the present study, we characterize spatial-temporal OGG1 DNA repair activity at telomeres of cancer cells during basal and oxidative stress conditions. Secondly, we explore whether OGG1 inhibition can interfere with BER activation at telomeres and characterize the telomere and cellular defects associated with OGG1 inhibition or depletion. Finally, we perform a screening for conventional chemotherapeutic agents that might synergize with OGG1 inhibitors contributing on telomere or genome instability.

METHODS

Cell culture and treatments

U2OS and BJ-TERT cells were cultured in DMEM (Lonza or Gibco) growth medium while NTUB1 and HCT116 were cultured in RPMI 1640 (Gibco) and McCoy's 5A Medium (Gibco), respectively. All cell line were supplemented with 10% of fetal bovine serum (Biowest) and 100 U/ml penicillin-streptomycin (Gibco) and grew at 37oC in a 5% CO2 atmosphere. To induce oxidative DNA damage, cells at about 80% of confluence were treated with H_2O_2 (Sigma) at 200µM in serum-free DMEM for the indicated periods. To perform OGG1 inhibition cells were released into fresh medium containing TH5487 (23) or DMSO (Sigma) for the indicated times and concentrations. After treatment, the cells were allowed to recover in complete growth medium for 1 h when mentioned. The different cell lines used for each experiment are detailed in Supplementary Table S1. Cell line authentication was performed by STR Profiling, and mycoplasma testing was performed regularly.

Plasmid construction OGG1-GFP and transfection

OGG1-GFP vector was generated according to the protocol described in Visnes *et al*., 2018 (23). U2OS cells were transfected with the vector using jetPEI (Polyplus) and selected with 1 ug/ml puromycin for 10 days. This was followed by clonal expansion to generate a single clone of U2OS cells constitutively expressing OGG1-GFP, and thus variability in expression levels was minimized.

CRISPR/Cas9 knockout of OGG1

sgRNAs were designed using the Benchling CRISPR sgRNA Design tool (*http://www.benchling.com*). A specific sgRNA was tested against *OGG1* gene and also a non-targeting control (NT) was used (sgOGG1#1: GTGTACTAGCGGATCAAGTA and sgNT: CCGCGCCGTTAGGGAACGAG). Those sequences were cloned into the lentiCRISPRv2 vector (Addgene plasmid #52961) and verified by Sanger sequencing.

Viruses were produced by transient plasmid transfection into 293T cells by the calcium phosphate method, as previously described (24). Briefly, cells were seeded at 1.1×10^7 cells/dish in 15-cm dishes the day before transfection. U2OS OGG1-GFP cells were transfected using second-generation packaging plasmids (psPAX2 and pMD.2G, Addgene #12260 and #12259, respectively) and the appropriate transfer plasmid (pLV CRISPR sgOGG1 or sgNT). The medium was collected after 48 h, cleared by low-speed centrifugation, and filtered through 0.45 µm-pore-size PVDF filters (Millipore). Viral titers were calculated and values range around 10^7 to 10^8 TU/ml. In order to carry out transductions, cells were split and 24 hours later were transduced using an MOI of 5 to ensure a high rate of transduced cells. Cells were incubated at 37ºC for 12 hours, and viral supernatant was replaced with fresh cell medium. A sorting step of the GFP negative cells was carried out to finally obtain the pool of cells were OGG1 knockout was validated by Western blot and IF (further detailed protocol).

Immunofluorescence microscopy and image analysis

U2OS cells were seeded in a 12-well plate for 24 h before the start of the indicated treatments and followed by the immunofluorescence protocol. Before fixation, cells were previously extracted with 0.2% Triton X-100 in PBS (Sigma) for 2 min (pre-extraction). Cells were fixed with 4% paraformaldehyde (PFA; Agar Scientific) for 10 min. After washing with PBS (Sigma), cell permeabilization was performed with

0.5% Triton X-100 (Sigma) in PBS for 15 min. Blocking with 3% Bovine Serum Albumin (BSA; Sigma) in PBS for 1 hour was followed by staining with primary and secondary antibodies and 0.5 µg/ml 4′,6-Diamidino-2-phenylindole dihydrochloride (DAPI; Sigma). After each staining, a washing step three times (10 minutes in PBS each time). Primary antibodies used were mouse anti-TRF2 (ab13579, Abcam) at 1/200, with antirabbit anti-γH2AX (2577S; Cell Signalling), anti-53BP1 (ab36823, Abcam) at 1/1,000, anti-XRCC1(ab134056; Abcam) at 1/200. Secondary antibodies: Anti-mouse Alexa 555 (TermoFisher Scientific), anti-rabbit Alexa 647 (TermoFisher Scientific). All steps were performed at room temperature. Image acquisition was performed with a Leica confocal microscope SP5 using ACS APO 40.0x1.15 OIL lens. Image treatment was done with Leica and ImageJ software and the analysis was performed using automatic CellProfiler software. For the analysis, we evaluated mean signal intensity within TRF2 foci for OGG1-GFP and XRCC1 (BER activation at telomere). For DNA damage markers γH2AX, and 53BP1, we measured overlapping index with the telomere marker TRF2. Finally, micronuclei frequency was calculated using cell profiler. All the experiments were performed at least 2 independent times. Data is available.

Telomere fluorescence *in situ* hybridization (FISH)

Cells were treated with 0.2 µg/ml Colcemide (Life Technologies) for 4 h to enrich cells at metaphase. Cell pellets were exposed to hypotonic treatment with 75 mM KCl solution, fixed in cold Carnoy's solution (methanol:acetic acid (3:1)), and spread onto glass slides. The samples were fixed again in PBS containing 3.7% paraformaldehyde and dehydrated by successive incubations in 70, 80, and 100% ethanol before FISH hybridization. DNA was denatured at 72ºC in 1M HCl, 20xSSC, and deionized formamide hybridization mixture, and hybridized with Cy3-labeled $(CCCTAA)_3$ peptide nucleic acid (PNA) telomere probe (0.5 µg/ml) (Panagene, PNA BIO/F1001 (TelC-FAM)). Finally, the slides were washed with a buffer containing the same high percentage of formamide to remove the nonspecifically bound probe, and DNA was stained with 0.5 µg/ml DAPI/Antifade solution (Palex Medical). Telomere FISH images were digitally acquired with a CCD camera (Photometrics SenSys) connected to a Leica DM5500B microscope using a 100x objective and using CytoVision software 7.2. Images were blinded analyzed to score for chromosome multitelomeric signal or signal-free ends.

Cell sorting

U2OS cells were trypsinized, resuspended at a concentration of 5×10^6 cells/ml and incubated with 5 µg/ml Hoechst for 15 min at 37°C in the dark. Cells were sorted based on the amount of DNA by defining three regions for sorting: G1, S, and G2/M phases. A post-sorting purity check was used to confirm the purities of the resulting sorted populations that were higher than 90% in all cases (Supplementary Figure S1A). The sorting was performed with the use of a BD Influx™ (BD Biosciences). The separated cells (at least 1×10^6 cells from each sorted population) were collected in tubes containing 0.5 ml culture medium and after centrifugation, cell pellets were stored at -20ºC until used for DNA or protein extraction.

Colony formation assay

U2OS cells (OGG1-GFP or OGG1-KO) with DMSO or with the indicated concentration of TH5487 were counted and seeded 10cm Petri dishes (500 cells per dish) and incubated until colony size surpassed a minimum of 50 cells (6 days). Then, the medium was removed and cells were challenged with a single pulse of OS H_2O_2 (Sigma) at 200µM in serum-free DMEM for 1h). Next, treatment was removed and cells placed in complete medium in the presence or absence of TH5487 (10µM) for 6 additional days. Finally, cells were washed twice with PBS, fixed with ice-cold methanol (Sigma) for 5 min, and stained with 1% crystal violet solution (Sigma) for 30 min. Following extensive washes in tap water and air drying. Plates were scanned and relative colony area was measured with ImageJ software. This experiment was performed once. Data is available.

DNA extraction, human OGG1 purification and relative quantification of oxidized bases in specific genome regions by qPCR

DNA was extracted from cultured cells using the Flexigene® DNA Kit (Qiagen) following the manufacturer's instructions and quantified by the PicoGreen® fluorometric assay (Thermo Fisher Scientific).

We have adapted the telomere oxidation protocol previously described (25) to quantify the relative accumulation of oxidized bases in specific genome regions by incubating the DNA with hOGG1protein, which was previously purified as previously reported (23). This is a qPCR method which is based on differences in PCR kinetics between template DNA digested by OGG1 and undigested DNA. This

enzyme recognizes and cuts 8-oxoG, producing abasic sites that are converted in SSBs by its AP lyase activity. These SSBs inhibit the PCR, thus, the ΔCt after digesting DNA by OGG1 (Ct digested–Ct undigested) is proportional to the oxidative damage in the amplified region (Supplementary Figure S1B). Conditions used for incubation were 2.4 μM hOGG1 for 4 h in DNA glycosylase buffer (25mM Tris-HCl, 15mM NaCl, 2mM MgCl2, 0.0025% Tween at pH=8). The reaction was stopped by incubating at 95ºC for 5 min. qPCR analysis was performed on 40 ng of digested or undigested genomic DNA using the same reagents, primers, and conditions as described in the original protocol (25). Each qPCR was performed in triplicate including no-template controls in an Abi QuantStudio 6 Flex Real-Time PCR System (Applied Biosystems) Primers used are listed in Supplementary Table S2. Six independent experiments were included for each condition and analyzed in triplicate. Data is available.

Protein extraction, quantification, and Immunoblotting

Protein expression was determined by immunoblotting. Briefly, cell pellets were prepared in RIPA buffer (Sigma) in the presence of a protease inhibitor cocktail (Roche). Total protein concentration was determined using the Pierce BCA Protein Assay Kit (Thermo Fisher Scientific) following the manufacturer's instructions. Forty micrograms of protein were electrophoresed on 12% SDS/PAGE and transferred to Immobilon-FL membranes (Millipore). Membranes were blocked in TBS-T (50 mM Tris/HCl, 150 mM NaCl, pH 7.5 plus 0.2% Tween-20) and 5% non-fat milk for 1 h at room temperature. Blots were probed with the following primary antibodies: rabbit anti-OGG1 (ab124741, Abcam) at 1/2,500 dilution, and mouse anti-β-actin (A5441; Sigma) at 1/10,000 dilution in TBS-T containing 5% non-fat milk. Anti-mouse and anti-rabbit IgG-HRP (Dako) were used as the secondary antibodies, and the immunoblots were developed using Immobilon Classico Western HRP substrate (Millipore). Each immunoblot was performed in triplicate. Images were analyzed using ImageJ software (NIH Image), and OGG1 protein level was normalized to actin levels. Original blots are not available.

Detection of intracellular ROS during cell cycle phases by flow cytometry

The generation of intracellular ROS during the cell cycle was determined using the fluorescent probe 2',7'-dichlorodihydrofluorescein diacetate (H2DCFDA; Molecular Probes) combined with Hoechst staining for detecting DNA content. The non-fluorescent H2DCFDA passively diffuses into cells and is converted

to the highly fluorescent 2',7'-dichlorofluorescein (DCF) upon oxidation by ROS. Cells were harvested using Trypsin (1X) for 5 minutes, pelleted and resuspended in PBS containing Hoechst (1µg/ml) for 15 minutes. Then, cells were washed with PBS and pelleted by centrifugation. Next, pellets were resuspended in RPMI without serum containing H2DCFDA to a final concentration of 10 µM, cells were incubated for 30 min at 37°C and analyzed by flow cytometry (Navios, Beckman Coulter) using the FL1 (525/540nm) or FL9 (450/460nm) channels. We used the median value of H2DCFDA intensity as a threshold to stratify negative (below median) or positive (above median) cells. Then, the percentage of ROS positive cells in G1, S, or G2M phases was calculated. This experiment was performed 2 independent times. Data is available.

Chromatin Immunoprecipitation

Chromatin Immunoprecipitation (ChIP) was performed as previously reported (26) in parental U2OS cells or U2OS cells expressing OGG1 protein fused to Green Fluorescence Protein (GFP). Chromatinized OGG1-GFP protein fraction was enriched by using GFP-Trap for Immunoprecipitation (IP) (Chromotek). DNA bound to OGG1-GFP was heated to reverse crosslinking. The purified OGG1-GFP DNA was amplified by PCR both telomere sequence and the single-copy gene *36B4* using specific primers (Supplementary Table S2). OGG1-GFP enrichment at telomeres or *36*B4 normalized to the 10% input was used to calculated the relative OGG1 enrichment for the 2 regions in U2OS-GFP cells compared to the parental U2OS cells. This experiment was performed 2 times. Data is available.

OGG1 target engagement

For sample preparation, cells were incubated with 20 µM TH5487 for 2 h at 37°C, (here is missing information: tripsinization, protein extraction, BCA,etc) before they were submitted for 3 min at twelve different temperatures ranging from 37°C to 62°C. After the addition of lysis buffer (50 mM Tris-HCl pH 7.5, 150 mM NaCl, 1 mM EDTA, 1% NP-40, 0.5% sodium deoxycholate and 0.1% SDS supplemented with complete protease inhibitor cocktail (Roche), cell lysis by freezing-thawing took place. In the following centrifugation (30 min at 17,000 g at 4°C) was performed and 70 µL of the supernatant was mixed with 23 µL loading dye before the samples were heated at 95 °C for 10 min. In the following, SDS-PAGE and WB were performed. The membrane was blocked with 5 % skimmed milk for 1 h at RT. As

primary antibodies rabbit anti-OGG1 (ab124741, Abcam) 1:1,000 and mouse anti-Actin (ab6276, Abcam) 1:5,000 were used. This experiment was performed once in U2OS cells (parental) and once in U2OS OGG1-GFP cells (not shown). Data is available.

Synergy experiments

Drug combinations were built and dispensed using D300e Digital Dispenser in 96 or 384 well plates. Cells were seeded in 96- or 384-well plates containing drug combinations by using Multidrop™ Combi Digital Dispenser. Then, cells were incubated for 3 days at 37C. Resazurin (R7017, Sigma) was added to a final concentration of 0.01 mg/ml resazurin and fluorescence was measured at ex530/em590 after incubation for 6 h in an HYDEX Sense microplate reader. Drug synergy Z-score was calculated and interpreted using Synergy Finder (*http://synergyfinder.fimm.fi*).

A preliminary synergy screening in U2OS, BJ-TERT, NTUB1, and HCT116 cells for TH5487 with conventional chemotherapeutic drugs (Cisplatin,5-Fluoracil, Doxorubicin, Methotrexate) or BER inhibitors (Olaparib, APE1i) was initiated for select the candidates. This initial screening was performed once. For the best candidates, Methotrexate and Doxorubicin synergies were repeated three independent times in four independent cell lines (U2OS, BJ-TERT, HCT116 and NTUB1).

Statistical analysis

The Kolmogorov–Smirnov test was used to evaluate whether the data sets were normally distributed. For comparative analyses, statistically significant differences were assessed by an unpaired t-test for normal distributions and the Mann–Whitney U-test for non-normal distributions. Statistical calculations and graphs were done using the SPSS software package version 19.0 (IBM) and GraphPad Prism 8 (GraphPad Software Inc).

RESULTS

Telomeres are a hotspot for oxidation due to cell cycle ROS production

We used the U2OS osteosarcoma cell line, a well-established model in telomere biology (27), for most experiments presented in this study. By using a modified version of the procedure described by

O'Callaghan et al. 2011 (25), we measured by qPCR oxidative DNA damage at telomeric DNA or the *36B4* locus, whose amplified regions contain a similar percentage of G:C base pairs (50% telomeres vs 52% *36B4*). In basal conditions, we found that U2OS cells accumulate higher levels of oxidized bases at telomeres compared to *36B4* locus (Figure 1A). Complementary, chromatin immunoprecipitation (ChIP) coupled to telomere PCR showed that OGG1 was significantly enriched at telomeres compared to the genomic region *36B4* in basal conditions (Figure 1B). Then, we measure oxidized bases levels in DNA from cells sorted by the cell cycle phase. In both genomic regions, the highest level of oxidative DNA damage was detected in the S phase (Figure 1C). The relative levels of telomeric oxidized bases between telomeres and the *36B4* locus (ΔCt ratio telomeres/36B4), were found during the G2/M phase (Supplementary Figure S1C).

Interestingly, OGG1 protein levels remained constant throughout the cell cycle in U2OS cells (Figure 1D). In contrast, when we measured intracellular ROS production during the cell cycle, we observed that in the transition from G1 to S phase, endogenous ROS levels increased until reaching maximum values during G2/M (Figure 1E), coinciding with the highest relative level of oxidized bases detected at telomeres. These results suggest that oxidative DNA damage generated by endogenous ROS might be progressively accumulated at the telomeres throughout the cell cycle.

OGG1 initiates BER at telomeres upon OS

In order to generate oxidative stress (OS) conditions, U2OS cells were exposed to H_2O_2 treatment (200 µM/1h). This treatment significantly increases oxidative lesions at telomeric DNA (Supplementary Figure S2A), demonstrating its efficacy. However, we measured OGG1 protein levels (Supplementary Figure S2B) under OS conditions, and no significant differences were detected compared to untreated cells.

Confocal microscopy in U2OS cells expressing OGG1 fused to GFP (OGG1-GFP) was used to follow whether OGG1 was recruited to damaged DNA after OS treatment. First, we removed the chromatin-unbound OGG1-GFP by using a pre-extraction step before fixation. Nuclear patches were detected only in cells exposed to OS, while in non-treated cells all the OGG1-GFP signal was removed (Supplementary Figures S2C and S2D). This result reflects the OGG1 recruitment to chromatin in response to oxidative DNA damage. Interestingly, suspension of OS treatment followed by a recovery period (fresh

medium/1h), caused a reduction in the levels of oxidized bases at telomeres (Supplementary Figure S2A), together with a significant decrease in OGG1-GFP recruitment to the DNA (Supplementary Figures S2C and S2D), evidencing the repair of oxidative lesions by BER. Furthermore, we measured by IF OGG1-GFP and XRCC1 signal intensity within Telomeric Repeat-binding Factor 2 (TRF2) foci (Supplementary Figures S2E – S2H). OS treatment significantly increases OGG1 and XRCC1 at TRF2 foci, providing evidences of BER activation at telomeres.

Pharmacological OGG1 inhibition disrupts BER at telomeres upon OS

The novel OGG1 inhibitor TH5487 has been reported to bind the active site of OGG1, blocking any potential interaction with its natural substrate (8-oxoG) in DNA (23). After showing that OGG1 is required to initiate BER at telomeres, we evaluated whether pharmacological inactivation of OGG1 using TH5487 can block BER at telomeres. Firstly, we confirmed that TH5487 engaged OGG1 in U2OS cells by thermal shift assay (Supplementary Figure S3A). Next, we challenged U2OS cells with TH5487 (10μM) and measured every 24h for 4 days, the level of oxidized bases at telomeres. We found that TH5487 led to a slow and progressive accumulation of oxidized bases at the telomere (Supplementary Figure S3B), likely derived from the ability of TH5487 to preclude OGG1 binding to the damaged telomeres (Supplementary Figure S3C).

Complementary, U2OS OGG1-GFP cells were used to generate a knockout for the *OGG1* gene by CRISPR/Cas9 (OGG1-KO, see material and methods). OGG1 knockout efficacy was validated by fluorescence microscopy and western blot (Supplementary Figures S3D and S3E). OGG1-KO U2OS cells were used to compare the effects at telomeres between OGG1 depletion and inhibition with TH5487. Similarly, to the treatment with the OGG1 inhibitor, OGG1-KO cells showed increased levels of oxidized bases at basal conditions at telomeres or *36B4* locus compared to U2OS-WT cells (Supplementary Figure S3F).

Additionally, we evaluated the ability of TH5487 of inhibiting the BER pathway at telomeres by Immunofluorescence (IF). Both in basal and upon OS treatment, OGG1 inhibition (TH5487) or depletion (OGG1-KO cells) resulted in a decrease of XRCC1 signal intensity at the telomere (Figures 2A and 2B), which reflects BER disruption at this specific region. In order to determine the consequences of BER

impairment, we measured in these cells the levels of oxidized bases at telomeric DNA by qPCR compared to the OGG1 proficient cells. We confirmed that OGG1 inhibition/depletion resulted in a higher accumulation of oxidative DNA damage at telomeres, particularly exacerbated upon OS (Figure 2C). Furthermore, a recovery period (fresh medium/1h) after OS treatment, which is coupled to a decrease in oxidative base lesions at telomeric DNA from U2OS proficient cells (Supplementary Figure S2A), did not alleviate oxidative DNA damage accumulation for those OGG1 inhibited or depleted cells (Figure 2C).

Finally, we measured the overlapping index of both DNA damage markers γH2AX and 53BP1 with TRF2 (telomere) by IF. We established 2 different OS conditions in the presence or absence of TH5487: for γH2AX we exposed cells to OS (H_2O_2 200uM/1h), while in the case of 53BP1 after an initial pulse of OS (H_2O_2 200uM/1h), we allowed cells to recover for 16h, since unrepaired SSBs generated via BER can be converted into DSBs after DNA replication (28). Upon oxidative conditions, we found a significantly increase in the overlapping index of both YH2AX and 53BP1 foci with telomere TRF2 foci. However, no significant differences were detected regarding OGG1 inhibition/depletion in basal or under OS conditions (Supplementary Figure S4).

Pharmacological OGG1 inhibition results in telomere losses and post-mitotic defects

To study the consequences of BER disruption at telomeres by OGG1 inhibition, we examined by telomere fluorescence *in situ* hybridization (Telo-FISH) whether TH5487 might compromise telomere integrity, or lead to post-mitotic abnormalities affecting cell proliferation. Analysis of metaphase chromosomes from U2OS OGG1-GFP cells revealed that 24h of exposure to TH5487 in U2OS was enough to observe a significant increase in telomere losses (signal-free ends) compared to the control treatment with DMSO. Similarly, OGG1-KO cells presented a higher number of telomere losses than U2OS-WT cells, and the TH5487 treatment did not cause additional telomere loses in these cells (Figures 3A and 3B). On the contrary, we did not observe significant differences in telomere fragility (multi-telomeric signal) after OGG1 depletion or inhibition at basal conditions (Figures 3A and 3C). Upon OS treatment, we could observe a significant increase in the frequency of chromosomes with multi-telomeric signals for both groups regardless of the OGG1 status, and no additional effect on the telomere losses (Supplementary

Figures S5A and S5B). These results suggest that telomere losses might be associated with OGG1 deficiency, while telomere fragility is a general phenotype occurring in OS conditions.

It has been previously reported that the accumulation of oxidative DNA damage induces replication stress at telomeres leading to post-mitotic defects, especially when OGG1 is knockout (16). Here, we measured micronuclei and chromosome bridge formation to evaluate whether the exposure to OS in OGG1 depleted or inhibited cells have effects on genomic stability. We found that OS caused a significant formation of micronuclei in both OGG1 proficient and deficient cells (Figure 3D). Interestingly, OGG1-KO cells or OGG1 proficient cells treated with TH5487 presented a significantly higher frequency of micronuclei regardless of OS conditions. In contrast, we were not able to find enough chromosome bridges to make a comparative analysis and only in OGG1-KO cells we could find them at a very low frequency (0.007).

Finally, we evaluated whether OGG1 inhibition or depletion could impair clonogenic potential in U2OS cells. No effect due to the OGG1 status was detected (Supplementary Figure S5C), reflecting that OGG1 inhibition/depletion is not enough to arrest cell proliferation in U2OS cells. Nevertheless, we found that when we inflicted OS conditions transiently during colony formation (H_2O_2 200uM/1h 6 days after seeding), OGG1 inhibition in combination with OS lead to the formation of smaller colonies compared to OGG1 proficient U2OS cells (p=0,06), a phenotype that was significantly more pronounced in the OGG1-KO cells (Figure 3E). These results indicate that upon OS conditions, OGG1 inhibition/depletion may lead to proliferation defects.

TH5487 synergizes with conventional anticancer drugs through induction of intracellular ROS, telomere DNA damage, and genome instability.

We carried out a screening study looking for potential synergies between OGG1 inhibitors and conventional chemotherapeutic drugs (Cisplatin,5-Fluoracil, Doxorubicin, Methotrexate) or other BER inhibitors (Olaparib, APE1i) which might potentiate some of the phenotypes described for TH5487 alone with an impact on cell viability for different human cell lines (U2OS, BJ-TERT, NTUB1, and HCT116).

First, we tested the effect on viability for different drug combinations during 72h in the different cell lines and calculated Synergy scores (Table 1). We found that for all the drugs/inhibitors tested, Methotrexate

(MTX) was the only compound that in combination with TH5487 presented a Z-score considered as a truly synergist (Z-Score>10, *https://synergyfinder.fimm.fi/*), for all tested cell lines (Table 1).

Next, based on the synergy maps generated with the viability data (Supplementary Figure S6), we selected sublethal doses within the synergy area for TH5487 (5-10 µM), and Methotrexate (10 µM) to evaluate the effect of each drug individually or in combination, for intracellular ROS generation, micronuclei formation, and 53BP1 foci overlapping index with TRF2 (telomeres). We first measured the intracellular ROS generated after 72h of exposure to MTX alone, or in combination with TH5487 in the 4 different cell lines (Figures 4B - 4E). Intracellular ROS formation by TH5487 was cell dependent. In contrast, MTX induced intracellular ROS formation in all cell lines tested at different levels. In combination with TH5487, only in NTUB1 and in HCT116 cell lines presented an additive interaction for intracellular ROS formation was detected (Figure 4). Next, we tested whether MTX alone or in combination with TH5487 could induce 53BP1-TIF or micronuclei formation in U2OS, BJ-TERT, and NTUB1. We excluded from the analysis HCT116 due to a lack of telomeric TRF2 foci detection by IF. In U2OS, TH5487 in combination with MTX caused the total effect (increased 53BP1/TRF2 overlapping index and increased micronuclei formation) to be greater than the sum of the individual effects of each drug, suggesting that TH5487 and MTX are synergistic drugs for these specific phenotypes (Figure 5).

In the case of NTUB1 cell line, MTX increased significantly 53BP1 and TRF2 overlapping index, and TH5487 potentiated the effect of MTX in an additive manner, while micronuclei formation remained unchanged with any drug combination (Supplementary Figures S7A and S7B). In contrast, neither 53BP1 foci formation at telomeres nor micronuclei formation were detected in BJ-TERT cells after exposure to TH5487 or MTX alone or in combination (Supplementary Figures S7C and S7D).

DISCUSSION

Telomeres and telomerase are key biological structures for supporting cancer cell proliferation since cancer cells can bypass the lifespan limits of normal cells by overexpressing telomerase (Telomerase +), or by using the alternative mechanism of telomere elongation (ALT+ cells). Hence, targeting telomeres or telomerase has been classically considered as a strategy for developing cancer therapies (7). In the present study, we have confirmed that TH5487 block BER initiation at telomeres in response to OS, and

we have characterized some of the TH5487 related telomeric and non-telomeric phenotypes in U2OS cells. Finally, we have tested different conventional chemotherapeutic agents in combination with TH5487, to identify potential synergistic drug combinations.

Even in basal conditions, we have found that telomeres are more prone to accumulate oxidative DNA damage than other genomic regions, especially during the S and G2/M cell cycle phases (Figure 1A and Figure S1C). This finding could be partially explained by, not only the progressive increase in intracellular ROS during the cell cycle (29,30), (Figure 1D) but also by the high condensation degree of telomeric chromatin during most cell cycle phases (31,32), since OGG1 does not operate on single-stranded or G4 contexts (16,33). In this regard, it has been recently reported that G4 folding occurs preferentially during G1/S and S-phases in U2OS cells (34). This correlates with the maximum peak in the intracellular ROS formation and with the accumulation of oxidative DNA damage detected at both genomic and telomeric regions, which might support a cell cycle control of BER through the chromatin accessibility via G4 folding/unfolding.

We used H_2O_2 to mimic OS conditions at telomeres (35) and confirmed a significant increase in oxidative base lesions in the telomeric DNA (Supplementary Figure S2D). Interestingly, OGG1 protein levels did not increase in response to OS (Supplementary Figure S2A) and also remained constant throughout the cell cycle, reflecting that *OGG1* expression is not cell-cycle regulated, or induced by oxidative DNA damage. However, we found that oxidative DNA damage accumulation at telomeres promoted the recruitment of BER enzymes in these regions to repair oxidized bases (Figure 2). These results suggest that, although OGG1 might behave as a housekeeping gene (36,37), it is actively recruited at telomeres in response to oxidative DNA damage to initiate BER. Our results, together with previous studies support the role of OGG1 as a key element promoting oxidative DNA damage repair at the telomere, via BER initiation (16,38–40).

Recently, the first example of cell-active inhibitors targeting OGG1 has been reported (23). Also details on how TH5487 binds to the human OGG1 sensitizing cancer cell lines by inducing replication stress without increasing nuclear 8oxoG levels (T.Visnes, *under review*). In relation with this, accumulation of 8oxodG

after TH5487 could be expected at guanine enriched regions such as gene promoters, 5', and 3' untranslated regions, or telomeres.

Indeed, here we found the following overlapping phenotypes between OGG1 depletion or inhibition in U2OS cells: First, a disruption in the recruitment of BER elements at telomeres during OS conditions (Figure 2), resulting in an accumulation of oxidized bases at this region (Supplementary Figure S3B). Although oxidative DNA lesions can potentially be converted into DSBs during BER (41), we were not able to detect telomere DNA damage response (DDR) because of OGG1 inactivation (Supplementary Figure S4). This result is supported by previous findings showing no DDR induction in OGG1 deficient cells (16) or a DDR restricted to cells undergoing replication after TH5487 in leukemic cells (T.Visnes, *under review*).

Second, we found that oxidative DNA damage at the telomere in OGG1 inactivated U2OS cells (depleted and/or TH5487), correlated with telomere losses and micronuclei formation (Figure 3B and Figure 3D). These phenotypes were also reported in Hela OGG1-KO cells in which chronic 8oxoG at telomeres induced telomere replication stress resulting in telomere crisis and the arrest of cell proliferation (16). In contrast, we detected minor proliferation defects related to OGG1 deficiency in combination with OS (Figure 3E). Since some telomerase negative cells correlate high basal levels of signal-free ends with telomere sister chromatid exchange (42), which is characteristic of ALT+ cancer cells, such as the U2OS cell line (43), it would be possible that telomere loss is well tolerated in these cells. And although we have recently proposed OGG1 as a potential anti-cancer target, and that TH5487 target a wide range of cancer cells (T.Visnes, *under review*), Depmap Public Database shows that cancer cell lines derived from bone, such as U2OS, present the lowest OGG1 cancer-dependency scores (DEMETER2; p=6.3*10-6) among lineages.

Finally, since TH5487 had a low impact on U2OS viability, we combined TH5487 with a heterogeneous set of conventional chemotherapeutic agents and BER inhibitors, looking for potential synergies in telomerase negative (U2OS) or positive transformed human cell lines (BJ-TERT, HCT116, NTUB1).

Despite PARP inhibitors targeting BER are known to induce replicative stress at telomeres to inhibit escape from a telomere crisis (44), we didn't find any synergy or additive effect with TH5487 (Table 1).

Indeed, it has been recently described that Olaparib toxicity in BRCA1-depleted cells is attenuated by treatments with a ROS scavenger, hypoxia, or OGG1 inhibitor (45), suggesting that toxicity derived from PARPi in cancer cells might be attenuated by BER inhibition.

Among the different conventional cancer drugs tested, we found Methotrexate to present the highest ZIP-synergy scores (Z-score >10 in the 4 tested cell lines). This drug has been reported to induce apoptosis through oxidative stress in rat small intestine (46), psoriasis patients (47), or lymphocytic T cells (48). In line with these findings, we showed that MTX induced intracellular ROS formation in all the cell lines we tested (Figure 4). Although MTX and TH5487 consistently synergized and correlated with intracellular ROS formation, the molecular mechanisms explaining the effects on cell viability for this drug combination were found to be cell type-specific and very little dependent on telomere instability or micronuclei formation in some cell lines, such as BJ-TERT, HCT116 or NTUB1.

On the other hand, we have reported that pharmacological inhibition of OGG1 with TH5487 might improve the anticancer properties of Methotrexate in U2OS cells, partially through an additive or synergistic increase of telomere DNA damage (53BP1 overlapping with TRF2) and genome instability (micronuclei formation) (Figure5), potentially associated with Methotrexate ROS induction. Supporting this, micronuclei formation in U2OS cells was found to increase during OS especially in OGG1 inhibited/depleted U2OS (Figure5C). In contrast, telomere DNA damage in U2OS cells after combining TH5487 and MTX (Figure 5A) might be independent on MTX ROS induction, since we didn't find additive effects on 53BP1-TIF formation when combined TH5487 with H2O2 (Supplementary Figure 4). Alternatively, this phenotype could be indirectly mediated by MTX folate metabolism (49) since MTX inhibits folic acid synthesis which has been reported to decrease intracellular ROS levels, telomeric DNA oxidative damage, and TIFs in astrocytes (50).

Combination therapies between TH5487 and MTX might be useful for those cancer types in which MTX is indicated such as breast cancer, acute lymphatic leukemia, lung cancer, lymphoma, and osteosarcoma (51). Besides cancer, there are some autoimmune diseases where MTX is used. This includes psoriasis, rheumatoid arthritis, and Crohn's disease (51). Methotrexate as a combination partner of TNF inhibitors induces high remission rates of rheumatoid arthritis (52) or superior drug survival in psoriatic arthrosis

patients receiving methotrexate co-medication with TNF-inhibitor (53). In this regard TH5487 is also known to prevent tumor necrosis factor-α-induced OGG1-DNA interactions that mediate TNF related pro-inflammatory gene expression (23). Hence, considering TH5487 as a "TNF-like inhibitor" we could expect some advantages of combination therapies in autoimmune diseases as well.

To conclude, our results show that TH5487 recapitulates some of the telomeric and post-mitotic defects previously reported in OGG1 KO cells (16). Therefore, OGG1 inhibitors can be considered as a new tool to block BER and to induce oxidative DNA damage at telomeres inducing cancer cell death, alone or in combination with other drugs like Methotrexate. This combination could be especially interesting to overcome Methotrexate resistance in cancer or autoimmune diseases (54,55).

CONCLUSIONS

Our data not only illustrate the importance of BER in DNA oxidative DNA damage repair at telomeres but also show the possible use of OGG1 inhibitor TH5487, enhances in combination with MTX, to induce telomere instability and proliferation defects, with potential implications in cancer treatment.

LIST OF ABBREVIATIONS

8-oxoG: 8-oxoguanine; BER: base excision repair; BSA: bovine serum albumine; DAPI: 4',6-diamidino-2-phenylindole; DCF: 2',7'-dichlorofluorescein; DDR: DNA damage response; DMEN: dulbecco's modified eagle medium; DMSO: dimethyl sulfoxide; EDTA: Ethylenediaminetetraacetic acid; FACS: fluorescence-activated cell sorting; FEN1: flap endonuclease 1; FISH: fluorescence in situ hybridization; GFP: green fluorescent protein; H2DCFDA: 2',7'-dichlorodihydrofluorescein diacetate; IF: immunofluorescence; IgG-HRP: immunoglobulin G horseradish peroxidase; KO: knockout; LIG1: DNA ligase 1; MOI: multiplicity of infection; MTX: Methotrexate; NT: non-targeting; OGG1: 8-oxoG DNA glycosylase 1; ORF: open reading frame; OS: oxidative stress; PARP: poly (ADP-ribose) polymerase; PBS: phosphate buffered saline; PFA: paraformaldehyde; PCNA: proliferating cell nuclear antigen; PCR: polymerase chain reaction; PVDF: polyvinylidene difluoride; PNA: peptide nucleic acid; POLB: polymerase beta; ROS: reactive oxygen species; SD: standard deviation; SDS-PAGE: sodium dodecyl sulfate–polyacrylamide gel electrophoresis; SEM: standard error of the mean; STR: short tandem repeat; TBS-T: tris buffered saline with tween 20;

TIF: telomere dysfunction-induced foci; TRF2: telomeric repeat-binding factor 2;T-SCE: Telomere sister chromatid exchange; WT: wild type;

DECLARATIONS

Ethics approval and consent to participate

Not applicable

Consent for publication

All authors have agreed to publish this manuscript. All materials and images are original. No consent needs to declare.

Availability of data and materials

The datasets used and analysed during the current study are available from the corresponding author upon reasonable request.

Competing interests

T.H. and T.V are listed as inventors on a provisional U.S. patent application no. 62/636983, covering OGG1 inhibitors. The patent is fully owned by a non-profit public foundation, the Helleday Foundation, and T.H., H.G. are members of the foundation board developing OGG1 inhibitors toward the clinic. The remaining authors declare no competing financial interests.

Funding

S.R.-P.'s laboratory is partially funded by funds from the Spanish National Research and Development Plan, Institute of Health Carlos III and FEDER (PI17/02303 to S.R-P). R.T.-R. is supported by a fellowship from the AECC scientific foundation. J.M.B. is supported by grant FPU15/01978 from the Spanish Ministry of Education, Culture and Sport. J.B.'s laboratory is partially funded by FIS PI16/00440 supported by FEDER funds, H2020 BRIDGES project and the Spanish Network on Rare Diseases (CIBERER). Vinnova (T.H.), the European Union's Horizon 2020 research and innovation program under the Marie Sklodowska-Curie grant agreement no. 722729 (T.H.), the European Research Council (T.H.), Swedish

Research Council (T.H.), Swedish Cancer Society (T.H.), the Swedish Children's Cancer Foundation (T.H.), and the Swedish Pain Relief Foundation (T.H.).

Authors' contributions

Study conception and design: J.B., C.B.-B., A.O. Acquisition of data: J.M.B., C.B.-B., Z.Z., R.T.-R., V.R., S.M., B.M.F.H. Analysis and interpretation of data: J.M.B., C.B.-B., J.B., A.O., S.R.-P. Drafting of manuscript: J.M.B., C.B.-B. Critical revision: J.B., A.O., O.L., O.W., M.M., H.G., T.V., T.H. All authors read and approved the final manuscript.

Acknowledgements

We thank Dr Diego Megias for assistance with image analysis, and Mónica Méndez for her contributions during early stages of the project.

REFERENCES

1. Blackburn EH. Switching and signaling at the telomere. Cell. 2001;106(6):661–73.
2. De Lange T. Shelterin: The protein complex that shapes and safeguards human telomeres. Genes Dev. 2005;19(18):2100–10.
3. Sfeir A, De Lange T. Removal of shelterin reveals the telomere end-protection problem. Science. 2012;336(6081):593–7.
4. Karlseder J. p53- and ATM-Dependent Apoptosis Induced by Telomeres Lacking TRF2. Science. 1999;283(5406):1321–5.
5. Longhese MP. DNA damage response at functional and dysfunctional telomeres. Genes Dev. 2008;22(2):125–40.
6. Maciejowski J, De Lange T. Telomeres in cancer: Tumour suppression and genome instability. Nat Rev Mol Cell Biol . 2017;18(3):175–86.
7. Ivancich M, Schrank Z, Wojdyla L, Leviskas B, Kuckovic A, Sanjali A, et al. Treating cancer by targeting telomeres and telomerase. Antioxidants. 2017;6(1).
8. Marnett LJ. Oxyradicals and DNA damage. Carcinogenesis. 2000;21(3):361–70.
9. Ahmed W, Lingner J. Impact of oxidative stress on telomere biology. Differentiation. 2018;99:21–7.
10. Barnes RP, Fouquerel E, Opresko PL. The impact of oxidative DNA damage and stress on telomere homeostasis. Mech Ageing Dev . 2019;177(February 2018):37–45.
11. Cadet J, Douki T, Ravanat JL. Oxidatively generated damage to the guanine moiety of DNA: Mechanistic aspects and formation in cells. Acc Chem Res. 2008;41(8):1075–83.
12. Le Page F, Guy A, Cadet J, Sarasin A, Gentil A. Repair and mutagenic potency of 8-oxoG:A and 8-oxoG:C base pairs in mammalian cells. Nucleic Acids Res. 1998;26(5):1276–81.

13. Opresko PL, Fan J, Danzy S, Wilson DM, Bohr VA. Oxidative damage in telomeric DNA disrupts recognition by TRF1 and TRF2. Nucleic Acids Res. 2005;33(4):1230–9.
14. Wang Z, Rhee DB, Lu J, Bohr CT, Zhou F, Vallabhaneni H, et al. Characterization of oxidative guanine damage and repair in mammalian telomeres. PLoS Genet. 2010;6(5):28.
15. Fouquerel E, Lormand J, Bose A, Lee HT, Kim GS, Li J, et al. Oxidative guanine base damage regulates human telomerase activity. Nat Struct Mol Biol . 2016;23(12):1092–100.
16. Fouquerel E, Barnes RP, Uttam S, Watkins SC, Bruchez MP, Opresko PL. Targeted and Persistent 8-Oxoguanine Base Damage at Telomeres Promotes Telomere Loss and Crisis. Mol Cell . 2019;75(May).
17. Von Morgen P, Maciejowski J. The ins and outs of telomere crisis in cancer. Genome Med. 2018;10(1):1–4.
18. Jia P, Her C, Chai W. DNA excision repair at telomeres. DNA Repair (Amst). 2015;36:137–45.
19. Fouquerel E, Parikh D, Opresko P. DNA damage processing at telomeres: The ends justify the means. DNA Repair (Amst) . 2016;44:159–68.
20. Svilar D, Goellner EM, Almeida KH, Sobol RW. Base excision repair and lesion-dependent subpathways for repair of oxidative DNA damage. Antioxidants Redox Signal. 2011;14(12):2491–507.
21. Krokan HE, Bjøra M. Base Excision Repair. Cold Spring Harb Perspect Biol. 2013;5:1–22.
22. Rhee DB, Ghosh A, Lu J, Bohr VA, Liu Y. Factors that influence telomeric oxidative base damage and repair by DNA glycosylase OGG1. DNA Repair (Amst) . 2011;10(1):34–44.
23. Visnes T, Cázares-Körner A, Hao W, Wallner O, Masuyer G, Loseva O, et al. Small-molecule inhibitor of OGG1 suppresses proinflammatory gene expression and inflammation. Science. 2018;362(6416):834–9.
24. Torres-ruiz R, Martinez-lage M, Martin MC, Garcia A, Bueno C, Castan J, et al. Efficient Recreation of t(11;22) EWSR1-FLI1+ in Human Stem Cells Using CRISPR/Cas9. Stem Cell Reports. 2017;8:1408–20.
25. O'Callaghan N, Baack N, Sharif R, Fenech M. A qPCR-based assay to quantify oxidized guanine and other FPG-sensitive base lesions within telomeric DNA. Biotechniques. 2011;51(6):403–12.
26. Carey MF, Peterson CL, Sinale ST. Chromatin Immunoprecipitation (ChIP). Cold Spring Harb Protoc. 2009;4(9):1–9.
27. Molenaar C, Wiesmeijer K, Verwoerd NP, Khazen S, Eils R, Tanke HJ, et al. Visualizing telomere dynamics in living mammalian cells using PNA probes. 2003;22(24):6631–41.
28. Schipler A, Iliakis G. DNA double-strand-break complexity levels and their possible contributions to the probability for error-prone processing and repair pathway choice. Nucleic Acids Res. 2013;41(16):7589–605.
29. Havens CG, Ho A, Yoshioka N, Dowdy SF. Regulation of Late G 1 / S Phase Transition and APC Cdh1 by Reactive Oxygen Species †. 2006;26(12):4701–11.

30. Patterson JC, Joughin BA, van de Kooij B, Lim DC, Lauffenburger DA, Yaffe MB. ROS and Oxidative Stress Are Elevated in Mitosis during Asynchronous Cell Cycle Progression and Are Exacerbated by Mitotic Arrest. Cell Syst . 2019;8(2):163-167.e2.
31. Galati A, Micheli E, Cacchione S. Chromatin Structure in Telomere Dynamics. Front Oncol. 2013;3(March):1–16.
32. Tardat M, Déjardin J. Telomere chromatin establishment and its maintenance during mammalian development. Chromosoma. 2018;127(1):3–18.
33. Zhou J, Liu M, Fleming AM, Burrows CJ, Wallace SS. Neil3 and NEIL1 DNA glycosylases remove oxidative damages from quadruplex DNA and exhibit preferences for lesions in the telomeric sequence context. J Biol Chem. 2013;288(38):27263–72.
34. Di Antonio M, Ponjavic A, Radzevičius A, Ranasinghe RT, Catalano M, Zhang X, et al. Single-molecule visualisation of DNA G-quadruplex formation in live cells. Nat Chem . 2020;1–6.
35. Coluzzi E, Colamartino M, Cozzi R, Leone S, Meneghini C, O'Callaghan N, et al. Oxidative stress induces persistent telomeric DNA damage responsible for nuclear morphology change in mammalian cells. PLoS One. 2014;9(10).
36. Dhénaut A, Boiteux S, Radicella JP. Characterization of the hOGG1 promoter and its expression during the cell cycle. 2000;461:109–18.
37. Mjelle R, Hegre SA, Aas PA, Slupphaug G, Drabløs F, Sætrom P, et al. Cell cycle regulation of human DNA repair and chromatin remodeling genes. DNA Repair (Amst) . 2015;30:53–67.
38. Campalans A, Amouroux R, Bravard A, Epe B, Radicella JP. UVA irradiation induces relocalisation of the DNA repair protein hOGG1 to nuclear speckles. J Cell Sci. 2007;120(1):23–32.
39. Amouroux R, Campalans A, Epe B, Radicella JP. Oxidative stress triggers the preferential assembly of base excision repair complexes on open chromatin regions. Nucleic Acids Res. 2010;38(9):2878–90.
40. Campalans A, Moritz E, Kortulewski T, Biard D, Epe B, Radicella JP. Interaction with OGG1 Is Required for Efficient Recruitment of XRCC1 to Base Excision Repair and Maintenance of Genetic Stability after Exposure to Oxidative Stress. Mol Cell Biol. 2015;35(9):1648–58.
41. Sharma V, Collins LB, Chen TH, Herr N, Takeda S, Sun W, et al. Oxidative stress at low levels can induce clustered DNA lesions leading to NHEJ mediated mutations. Oncotarget. 2016;7(18):25377–90.
42. Wang Y, Erdmann N, Giannone RJ, Wu J, Gomez M, Liu Y. An increase in telomere sister chromatid exchange in murine embryonic stem cells possessing critically shortened telomeres. Proc Natl Acad Sci U S A. 2005;102(29):10256–60.
43. Londoño-Vallejo JA, Der-Sarkissian H, Cazes L, Bacchetti S, Reddel RR. Alternative Lengthening of Telomeres Is Characterized by High Rates of Telomeric Exchange. Cancer Res. 2004;64(7):2324–7.

44. Ngo G, Hyatt S, Grimstead J, Jones R, Hendrickson E, Pepper C, et al. PARP inhibition prevents escape from a telomere-driven crisis and inhibits cell immortalisation. Oncotarget. 2018;9(101):37549–63.
45. Giovannini S, Weller MC, Repmann S, Moch H, Jiricny J. Synthetic lethality between BRCA1 deficiency and poly(ADP-ribose) polymerase inhibition is modulated by processing of endogenous oxidative DNA damage. Nucleic Acids Res. 2019;47(17):9132–43.
46. Miyazono Y, Gao F, Horie T. Oxidative stress contributes to methotrexate-induced small intestinal toxicity in rats. Scand J Gastroenterol. 2004;39(11):1119–27.
47. Elango T, Dayalan H, Gnanaraj P, Malligarjunan H, Subramanian S. Impact of methotrexate on oxidative stress and apoptosis markers in psoriatic patients. Clin Exp Med. 2014;14(4):431–7.
48. Herman S, Zurgil N, Deutsch M. Low dose methotrexate induces apoptosis with reactive oxygen species involvement in T lymphocytic cell lines to a greater extent than in monocytic lines. Inflamm Res. 2005;54(7):273–80.
49. Shao Y, Tan B, Shi J, Zhou Q. Methotrexate induces astrocyte apoptosis by disrupting folate metabolism in the mouse juvenile central nervous system. Toxicol Lett . 2019;301:146–56.
50. Li W, Ma Y, Li Z, Lv X, Wang X, Zhou D, et al. Folic acid decreases astrocyte apoptosis by preventing oxidative stress-induced telomere attrition. Int J Mol Sci. 2020;21(1).
51. Abolmaali SS, Tamaddon AM, Dinarvand R. A review of therapeutic challenges and achievements of methotrexate delivery systems for treatment of cancer and rheumatoid arthritis. Cancer Chemother Pharmacol. 2013;71(5):1115–30.
52. Witte T. Methotrexate as combination partner of TNF inhibitors and tocilizumab. What is reasonable from an immunological viewpoint? Clin Rheumatol. 2015;34(4):629–34.
53. Fagerli KM, Lie E, Van Der Heijde D, Heiberg MS, Lexberg ÅS, Rødevand E, et al. The role of methotrexate co-medication in TNF-inhibitor treatment in patients with psoriatic arthritis: Results from 440 patients included in the NOR-DMARD study. Ann Rheum Dis. 2014;73(1):132–7.
54. Guo W, Healey JH, Meyers PA, Ladanyi M, Huvos AG, Bertino JR, et al. Mechanisms of methotrexate resistance in osteosarcoma. Clin Cancer Res. 1999;5(3):621–7.
55. Johnson KJ, Sanchez HN, Schoenbrunner N. Defining response to TNF-inhibitors in rheumatoid arthritis: the negative impact of anti-TNF cycling and the need for a personalized medicine approach to identify primary non-responders. Clin Rheumatol. 2019;38(11):2967–76.

FIGURE LEGENDS

Figure 1 Telomeres are a hotspot for oxidation due to cell cycle ROS production. (A) DNA from U2OS cells was used to measure 8-oxoG levels at the 36B4 locus or telomeric DNA. Bars show the mean and the standard error of the mean (SEM) from 3 technical replicates from 6 independent experiments for each condition (Mann-Whitney test; **P<0.01). (B) OGG1-GFP pulldown followed by chromatin immunoprecipitation coupled to PCR for amplification of either 36B4 locus or the telomere regions in the U2OS parental and U2OS OGG1-GFP cell lines. Data are the average of 3 technical replicates from 2 independent experiments. Statistical significance was determined using (Mann-Whitney test; **P<0.01. (**C**) Sorted DNA from different cell cycle phases (G1, S, or G2/M) from U2OS cells was used to evaluate 8-oxoG levels at the *36B4* locus or telomeric DNA along the cell cycle. Bars show the mean and the SEM from 3 technical replicates from 6 independent experiments for each condition (two-sided T-test; *** P<0.001). (**D**) Quantification of OGG1 protein expression level in U2OS cells along the cell cycle. Actin levels were used to normalize for protein loading. Immunoblot was performed in triplicate (two-sided T-test). (**E**) Percentage of cells with intracellular ROS levels above the median of the whole U2OS population is represented in different cell cycle stages (G1, S, or G2/M). Data are average ±SEM from single measures from 2 independent experiments. Significant differences were addressed by two-sided T-test (P<0.05, ns).

Figure 2: Pharmacological OGG1 inhibition disrupts BER at telomeres upon OS. (**A**) Confocal imaging of XRCC1 (red) and TRF2 (green) by immunofluorescence using specific antibodies. DAPI was used to stain the cell nucleus (blue). (**B**) Quantification of XRCC1 signal intensity integrated within telomeres from more than 200 foci per condition. Data are the average with SEM from 2 independent experiments (Mann-Whitney test; **** P<0.0001). (**C**) Relative level of oxidized bases at telomeres in OGG1 inhibited/depleted U2OS cells upon oxidative stress treatment (H_2O_2 200µM/1h) or followed by a recovery period (fresh media/1h). Bars show the mean and the SEM from 3 technical replicates from 6 independent experiments for each condition (two-sided T-test; *** P<0.001).

Figure 3: **Pharmacological OGG1 inhibition results in telomere losses and post-mitotic defects.** (**A**) Representative TELO-FISH images of an unaltered chromosome in metaphase stained with DAPI (in

blue) with the corresponding telomeric signals (in green) at the end of each chromatid. Below, Representative TELO-FISH images of altered chromosomes showing telomere signal loss in one of the chromatids, multi-telomeric signals, and a micronucleus (orange arrows). (**B**) Quantification of telomeric signal-free ends for the indicated conditions in U2OS-WT or OGG1-KO cells. Bars show the mean and the standard error of the mean (SEM) for frequency events/metaphase (30 to 35 metaphases per condition from 2 independent experiments). Statistical significance was determined using unpaired, two-sided T-tests (**P<0.01 and ***P<0.001). (**C**) Comparative analysis of the frequency of multi-telomeric signals for the indicated conditions in U2OS-WT or OGG1-KO cells. Bars show the mean and the standard error of the mean (SEM) for frequency events/metaphase (30 to 35 metaphases per condition from 2 independent experiments). Statistical significance was determined using unpaired, two-sided T-tests. (**D**) Comparative analysis of micronuclei formation frequency for U2OS-WT incubated with DMSO or TH5487 and for OGG1-KO at basal condition or during OS. More than 200 cells per condition were analyzed. Data is the average of 2 independent experiments. Significant differences were calculated using the Mann-Whitney test for non-parametric distributions (**P<0.01 , ***P<0.001, **** P<0.0001). (**E**) Up, comparative analysis for the colony area generated in each condition. Significant differences were calculated using Mann-Withney test for non-parametric distributions (**** P<0.0001). Down, summary for the schedule of treatment to evaluate a specific clonogenic potential feature (area of colonies). Data are average of the mean colony area values of a single experiment.

Figure 4: Intracellular ROS formation. (**A**) Intracellular ROS (H2DCFDA mean intensity) generated after 72h of exposure to MTX (10 µM), alone or in combination with 10 µM TH5487 in U2OS cells, (**B**) BJ-TERT, (**C**) NTUB1 or (**D**) HCT116 cells. Except for NTUB1 in combination TH5487/MTX, that TH5487 was used at 5µM. Data are average and SEM of single measurements from 2 independent experiments. Statistics were excluded from this analysis due to the low amount of data points to establish relevant comparation between groups.

Figure 5 TH5487 synergizes with methotrexate through induction of telomere DNA damage, and genome instability. (**A**) Quantification of 53BP1 signal intensity integrated within telomeres from more than 200 U2OS cells per condition. Data are the average with SEM from 2 independent experiments.

Significant differences were calculated using Mann-Withney test for non-parametric distributions (**** p<0.0001). (**B**) Confocal imaging at single U2OS cells representative for each treatment condition and stained for 53BP1 (red) and TRF2 (green) using specific antibodies or DAPI to stain cell nucleus (blue).(**C**) Comparative analysis of micronuclei formation frequency for U2OS incubated with MTX (10 µM) for 72h, alone or in combination with TH5487 (10µM) in U2OS cells. More than 200 cells per condition were analyzed. Data is the average of 2 independent experiments. Significant differences were calculated using the Mann-Whitney test for non-parametric distributions (**** p<0.0001).

TABLES

Table 1. ZIP synergy scores for conventional chemotherapeutic drugs or BER inhibitors in combination with TH5487

Cell line	Methotrexate	Doxorubicin	5-Fluoracil	APE1i	PARPi	Cisplatin
HCT116	10.77	4.97	5.33	3.55	3.09	2.84
NTUB1	48.56	5.84	-3.09	3.05	3.28	-14.97
U2OS	11.36	2.891	0.5	-2.57	1.97	-13.28
BJ-TERT	21.	5.88	-	-	-7.46	-

Figures

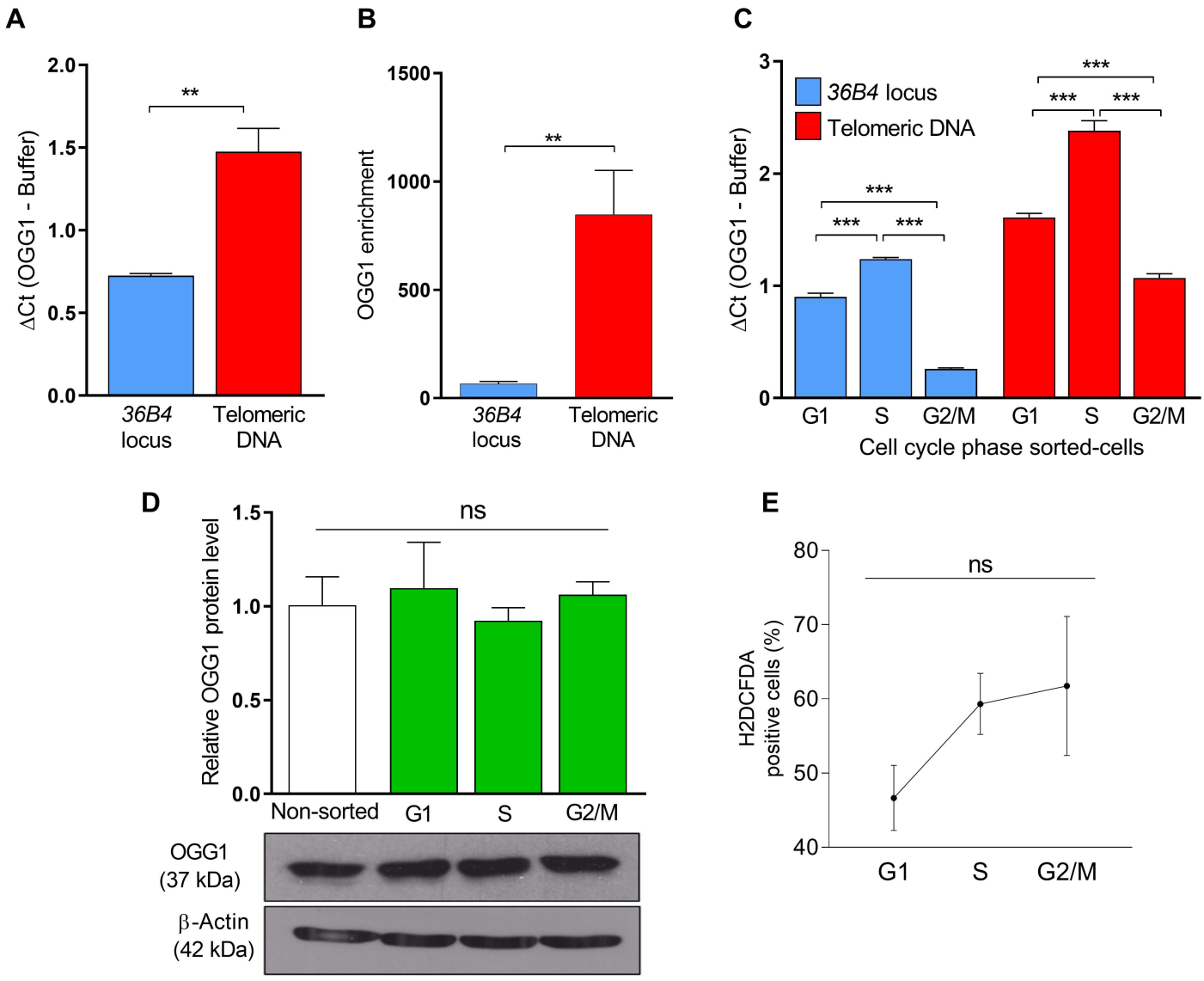

Figure 1

Telomeres are a hotspot for oxidation due to cell cycle ROS production. (A) DNA from U2OS cells was used to measure 8-oxoG levels at the 36B4 locus or telomeric DNA. Bars show the mean and the standard error of the mean (SEM) from 3 technical replicates from 6 independent experiments for each condition (Mann-Whitney test; **P<0.01). (B) OGG1-GFP pulldown followed by chromatin immunoprecipitation coupled to PCR for amplification of either 36B4 locus or the telomere regions in the U2OS parental and U2OS OGG1-GFP cell lines. Data are the average of 3 technical replicates from 2 independent experiments. Statistical significance was determined using (Mann-Whitney test; **P<0.01. (C) Sorted DNA from different cell cycle phases (G1, S, or G2/M) from U2OS cells was used to evaluate 8-oxoG levels at the 36B4 locus or telomeric DNA along the cell cycle. Bars show the mean and the SEM from 3 technical replicates from 6 independent experiments for each condition (two-sided T-test; *** P<0.001). (D)

Quantification of OGG1 protein expression level in U2OS cells along the cell cycle. Actin levels were used to normalize for protein loading. Immunoblot was performed in triplicate (two-sided T- test). (E) Percentage of cells with intracellular ROS levels above the median of the whole U2OS population is represented in different cell cycle stages (G1, S, or G2/M). Data are average ±SEM from single measures from 2 independent experiments. Significant differences were addressed by two-sided T- test (P<0.05, ns).

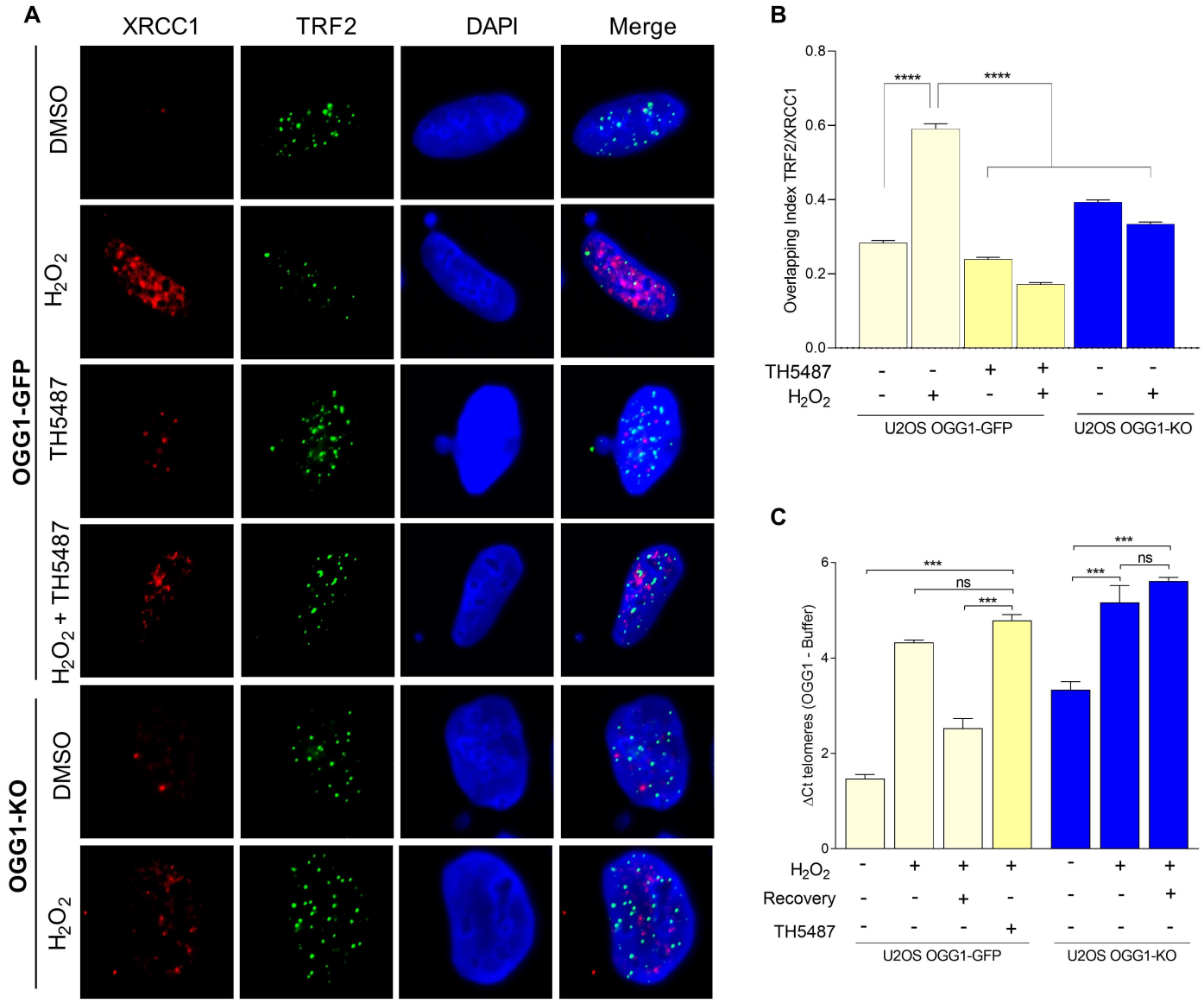

Figure 2

Pharmacological OGG1 inhibition disrupts BER at telomeres upon OS. (A) Confocal imaging of XRCC1 (red) and TRF2 (green) by immunofluorescence using specific antibodies. DAPI was used to stain the cell nucleus (blue). (B) Quantification of XRCC1 signal intensity integrated within telomeres from more than 200 foci per condition. Data are the average with SEM from 2 independent experiments (Mann-Whitney test; **** P<0.0001). (C) Relative level of oxidized bases at telomeres in OGG1 inhibited/depleted U2OS cells upon oxidative stress treatment (H2O2 200µM/1h) or followed by a recovery period (fresh

media/1h). Bars show the mean and the SEM from 3 technical replicates from 6 independent experiments for each condition (two-sided T-test; *** P<0.001).

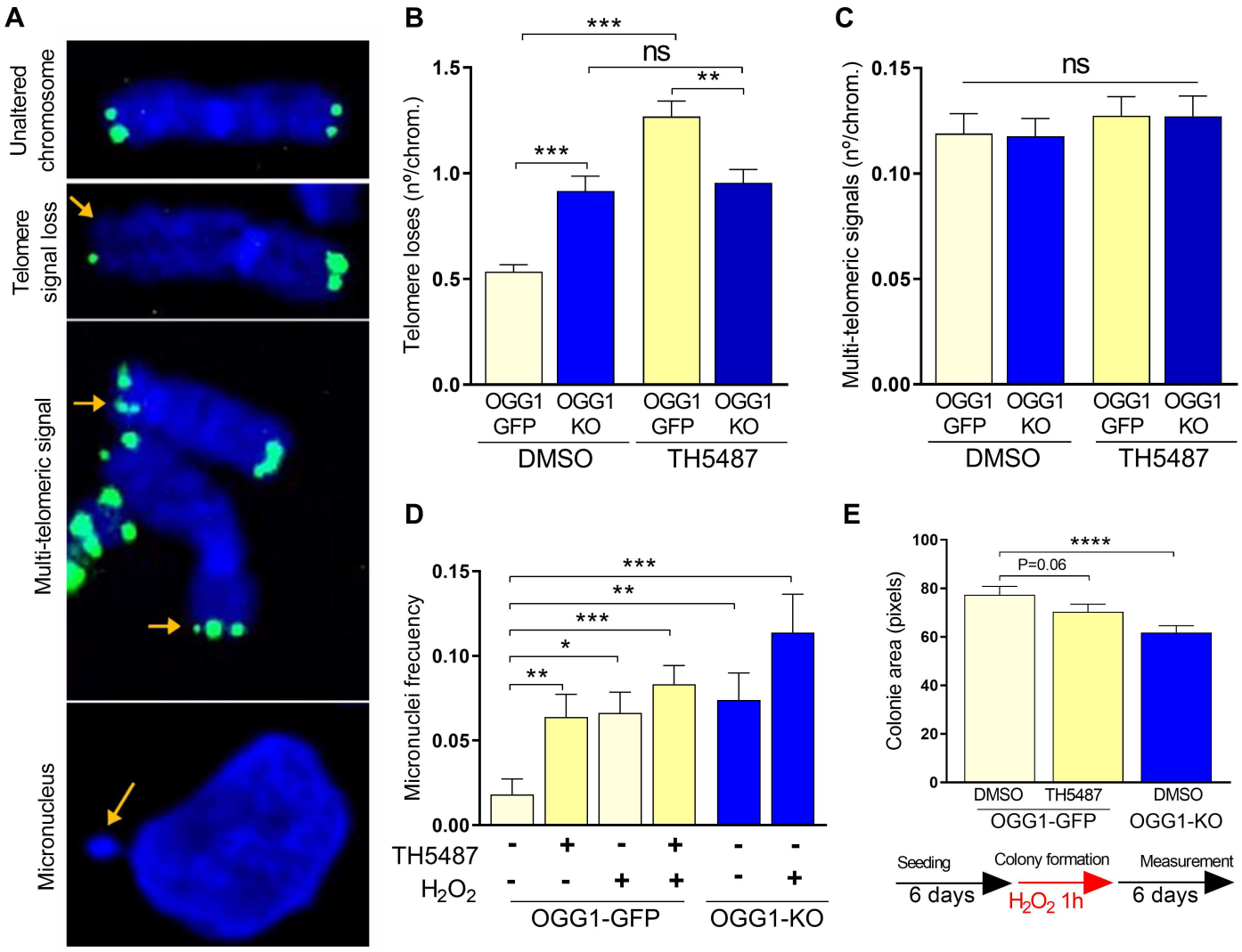

Figure 3

Pharmacological OGG1 inhibition results in telomere losses and post-mitotic defects. (A) Representative TELO-FISH images of an unaltered chromosome in metaphase stained with DAPI (in blue) with the corresponding telomeric signals (in green) at the end of each chromatid. Below, Representative TELO-FISH images of altered chromosomes showing telomere signal loss in one of the chromatids, multi-telomeric signals, and a micronucleus (orange arrows). (B) Quantification of telomeric signal-free ends for the indicated conditions in U2OS-WT or OGG1-KO cells. Bars show the mean and the standard error of the mean (SEM) for frequency events/metaphase (30 to 35 metaphases per condition from 2 independent experiments). Statistical significance was determined using unpaired, two- sided T-tests (**P<0.01 and ***P<0.001). (C) Comparative analysis of the frequency of multi-telomeric signals for the indicated conditions in U2OS-WT or OGG1-KO cells. Bars show the mean and the standard error of the mean (SEM) for frequency events/metaphase (30 to 35 metaphases per condition from 2 independent

experiments). Statistical significance was determined using unpaired, two-sided T- tests. (D) Comparative analysis of micronuclei formation frequency for U2OS-WT incubated with DMSO or TH5487 and for OGG1-KO at basal condition or during OS. More than 200 cells per condition were analyzed. Data is the average of 2 independent experiments. Significant differences were calculated using the Mann-Whitney test for non-parametric distributions (**P<0.01 , ***P<0.001, **** P<0.0001). (E) Up, comparative analysis for the colony area generated in each condition. Significant differences were calculated using Mann-Withney test for non-parametric distributions (**** P<0.0001). Down, summary for the schedule of treatment to evaluate a specific clonogenic potential feature (area of colonies). Data are average of the mean colony area values of a single experiment.

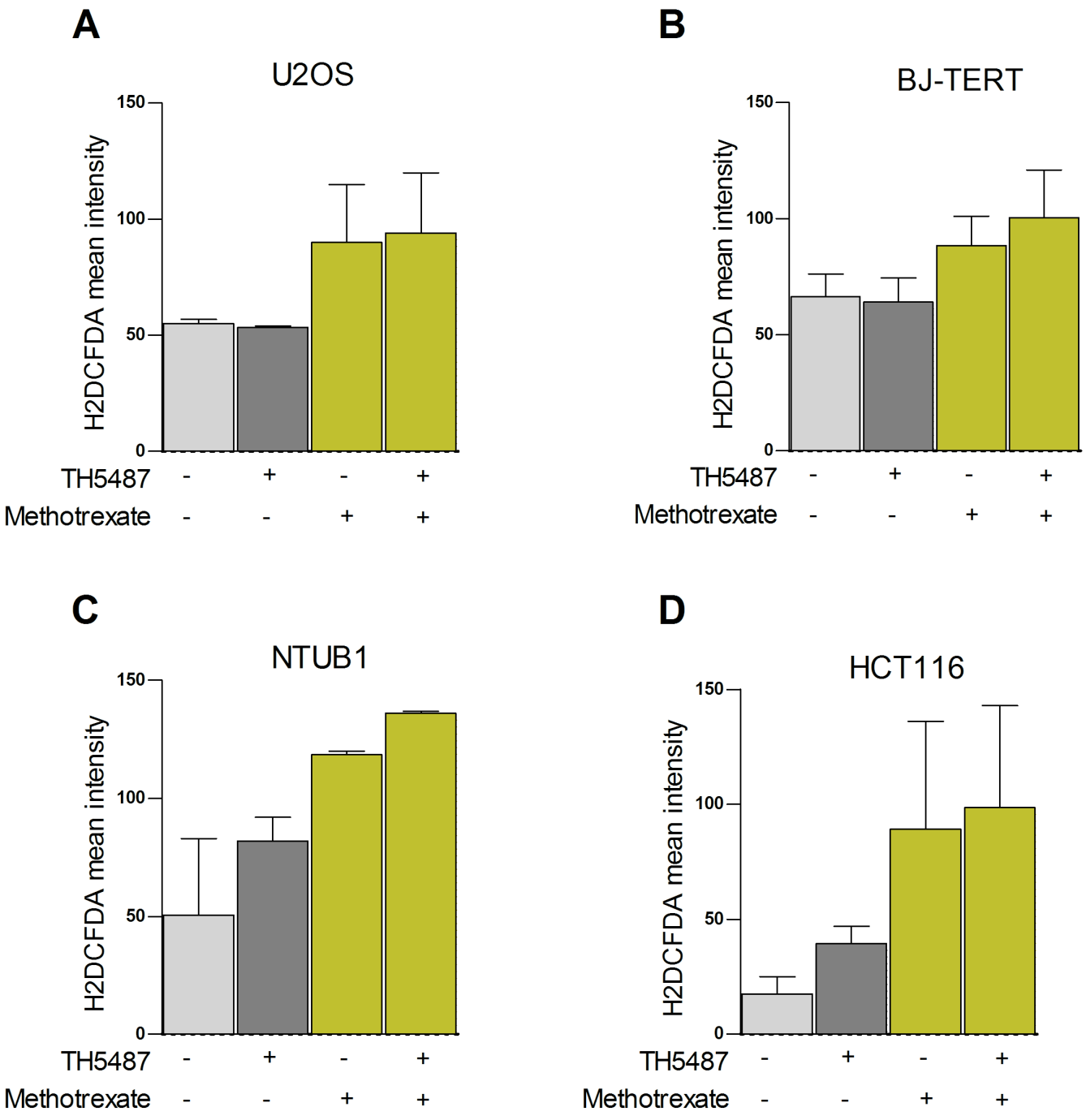

Figure 4

Intracellular ROS formation. (A) Intracellular ROS (H2DCFDA mean intensity) generated after 72h of exposure to MTX (10 μM), alone or in combination with 10 μM TH5487 in U2OS cells, (B) BJ-TERT, (C) NTUB1 or (D) HCT116 cells. Except for NTUB1 in combination TH5487/MTX, that TH5487 was used at 5μM. Data are average and SEM of single measurements from 2 independent experiments. Statistics were excluded from this analysis due to the low amount of data points to establish relevant comparation between groups.

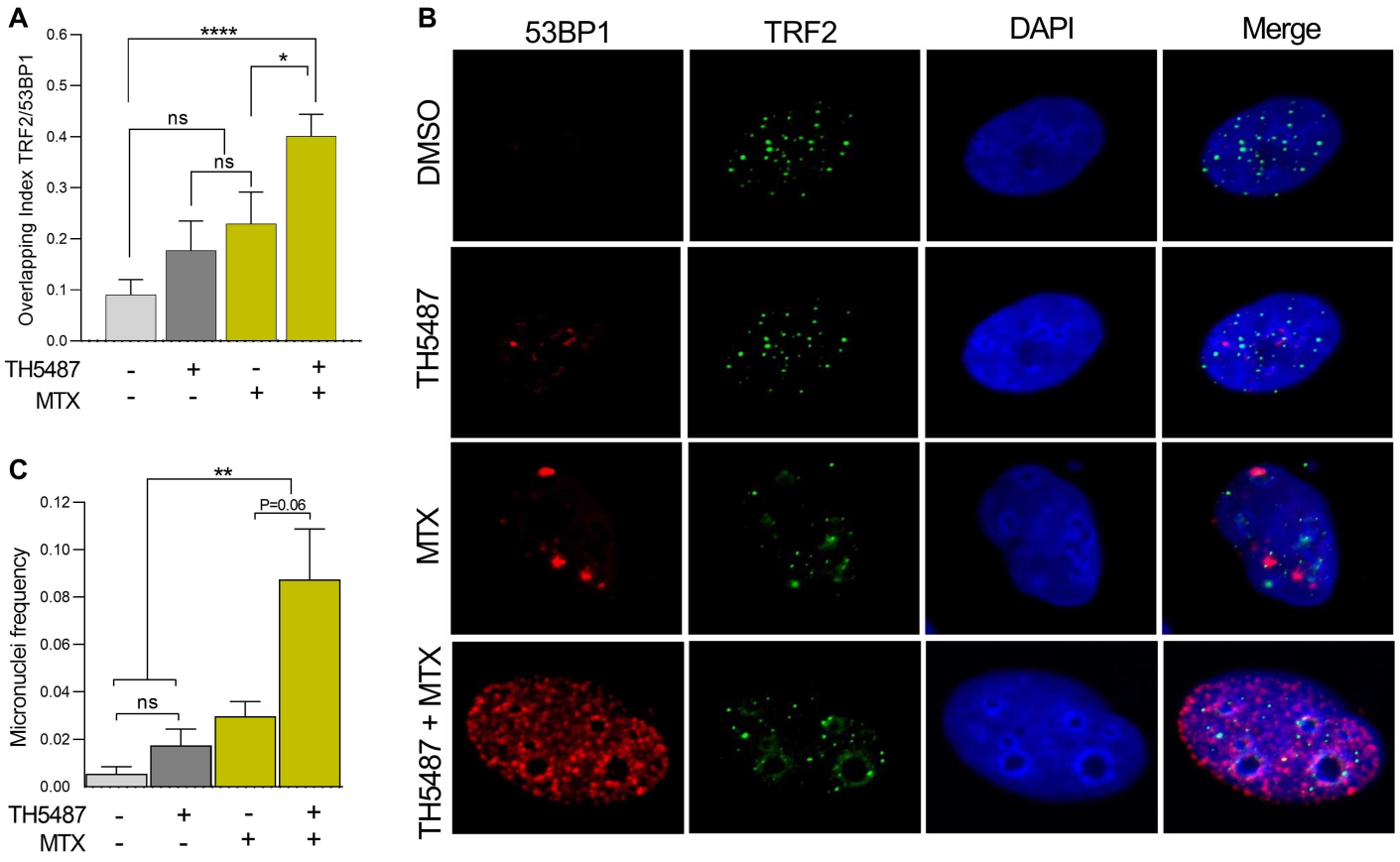

Figure 5

TH5487 synergizes with methotrexate through induction of telomere DNA damage, and genome instability. (A) Quantification of 53BP1 signal intensity integrated within telomeres from more than 200 U2OS cells per condition. Data are the average with SEM from 2 independent experiments. Significant differences were calculated using Mann-Withney test for non-parametric distributions (**** p<0.0001). (B) Confocal imaging at single U2OS cells representative for each treatment condition and stained for 53BP1 (red) and TRF2 (green) using specific antibodies or DAPI to stain cell nucleus (blue).(C) Comparative analysis of micronuclei formation frequency for U2OS incubated with MTX (10 μM) for 72h, alone or in combination with TH5487 (10μM) in U2OS cells. More than 200 cells per condition were analyzed. Data is the average of 2 independent experiments. Significant differences were calculated using the Mann-Whitney test for non-parametric distributions (**** p<0.0001).

Supplementary Files

This is a list of supplementary files associated with this preprint. Click to download.

- SupplementaryData.pdf